JMJD3 Deficiency in Midbrain Dopamine Neurons Disrupts Dopamine Synthesis and Aggravates Chronic Inflammatory Pain.

Running title: JMJD3, dopamine and chronic pain.

Xi-Biao He[1,*], Fang Guo[1,#], Wei Zhang[2,#], Weidong Le[3], Yong Zheng[1,4], Yongjun Ma[1,4], Hui-Jing Wang[5], Yi Wu[1,&], Qinming Zhou[6].

[1] Laboratory of Stem Cell Biology and Epigenetics, School of Basic Medical Sciences, Shanghai University of Medicine and Health Sciences, Shanghai 201318, China.

[2] State Key Laboratory of Microbial Metabolism, School of Life Science and Biotechnology, Shanghai Jiao Tong University, Shanghai 200240, China.

[3] Center for Translational Medicine, Shanghai University of Medicine and Health Sciences, Shanghai 201318, China.

[4] School of Pharmacy, Shanghai University of Medicine and Health Sciences, Shanghai 201318, China.

[5] Laboratory of Neuropsychopharmacology, School of Basic Medical Sciences, Shanghai University of Medicine and Health Sciences, Shanghai 201318, China.

[6] Department of Neurology, Ruijin Hospital, Shanghai Jiao Tong University School of Medicine, Shanghai 200025, China.

# These authors contribute equally to this work.

& Current address: Institute of Neuroscience, State Key Laboratory of Neuroscience, CAS Center for Excellence in Brain Science and Intelligence Technology, Chinese

Academy of Sciences, Shanghai 200031, China.

* Corresponding author

Xi-Biao He

Address: 279 Zhouzhu Highway, Pudong New Area, Shanghai, 201318, China

Tel: 86-18516097628

E-mail: hexb@sumhs.edu.cn

Abstract

Chronic pain is associated with midbrain dopamine levels. The molecules and underlying mechanisms modulating this association remain to be elucidated. By using conditional knockdown mice, we report that JMJD3 deficiency in midbrain dopamine neurons causes prolonged mechanical hyperalgesia regardless of sex and age. Both genetic loss and pharmaceutical inhibition of JMJD3 decrease dopamine level in midbrain and striatum, resulting from reduced tyrosine hydroxylase expression in midbrain dopamine neurons. Furthermore, epigenetic experiments reveal that JMJD3 is indispensable for the transcription of tyrosine hydroxylase. These findings suggest JMJD3 and midbrain dopamine neurons as novel players and pharmaceutical targets for chronic pain regulation.

Key words: Midbrain dopamine neuron; JMJD3; Tyrosine hydroxylase; Chronic pain; Epigenetics

Introduction

Dopamine (DA) neurotransmission is widely implicated in the modulation of pain (1, 2). Midbrain DA neurons of the ventral tegmental area (VTA) and substantia nigra pars compacta (SNc) are the major cell types that produce DA in the central nervous system. Increasing evidence indicate a strong association between chronic pain and decreased DA activities in midbrain DA neurons (3–8), whereas the regulatory molecules and underlying mechanisms are much less understood.

Tyrosine hydroxylase (TH) is the rate-limiting enzyme for DA biosynthesis, which is down-regulated in pathological midbrain DA neurons in Parkinson's disease (PD) (9). Although chronic pain is a common non-motor symptom in PD patients (10), whether decreased TH activity plays a causal role in PD-related pain hyperactivity remains unclear. Depending on cellular context, TH expression and activity are epigenetically, transcriptionally and post-translationally regulated (11). Despite of a large number of transcription factors identified (12), the epigenetic factors that affect TH-mediated DA synthesis are just beginning to get revealed.

Jumonji C-domain-containing histone deacetylase 3 (JMJD3) is a histone deacetylase specifically demethylating histone 3 lysine 27 (H3K27), which is related to chromatin remodeling that switches transcription from repression to activation (13). JMJD3 participates in a wide range of biological processes in various types of cells, from early embryonic development to cell senescence (14). However, little is known about the roles of JMJD3 in midbrain DA neurons, except for our previous study reporting it as an indispensable transcription factor for the DA phenotype commitment of prenatal DA progenitor cells (15).

To understand the role of JMJD3 in adult midbrain DA neurons, we have constructed DA neuron-specific JMJD3 conditional knockdown mice and investigated the how JMJD3 deficiency affects midbrain DA neurons on molecular, cellular and behavioral levels.

Results & Discussion

Th-specific *Jmjd3* knockdown exaggerates chronic inflammatory pain.

We created a conditional knockdown (cKD) mouse model by crossbreeding transgenic mice carrying *Th*-CRE and loxP-floxed *Jmjd3* loci, respectively. Offspring mice carrying *Th*-CRE and one allele of loxP-floxed *Jmjd3* were used as cKD and those carrying *Th*-CRE and normal *Jmjd3* as control (WT; Supplemental Fig. S1A). To understand the behavioral phenotype of this model, WT and cKD mice in different sexes and ages underwent inflammation-induced mechanical hyperalgesia test and accelerating rotarod test respectively, to determine their pain sensitivity and locomotor coordination, both of which are midbrain DA-related.

To induce mechanical hyperalgesia, complete Freund's adjuvant (CFA) was injected intraplantarly in both WT and cKD mice. Pain sensitivity was measured at various time points over 18 days by Von Frey's hairs. As expected, WT and cKD mice showed no difference in basal nociception. CFA caused significant pain hypersensitivity over the first three hours, regardless of sex and age, indicating an intact perception of acute pain for this mouse model (Fig. 1A-D). The pain sensitivity was not attenuated until the eighth day (D8) in both male and female young WT mice, followed by a nearly complete recovery from D13, validating the confidence of this test. By contrast, the hyperalgesia lasted for at least 13 days in young cKD mice of both sexes, and was only slightly attenuated at D18 (Fig. 1A, B). This result indicated a sex-independent prolonged pain hypersensitivity in young cKD mice. On the other hand, the hyperalgesia was not attenuated in old male WT mice, and to a much milder extent in old female ones over 18 days (Fig. 1C, D), suggesting that the pain maintenance was worsened along aging. In comparison, similar to young cKD mice,

neither old male nor female cKD mice showed attenuation of hyperalgesia over 18 days. These results demonstrated that conditional *Jmjd3* knockdown caused age- and sex-independent pain maintenance. To confirm the pain specificity, the thermal hyperalgesia was measured in parallel using a Hargreaves method (16) and no difference was observed (Supplemental Fig. S1B).

The accelerating rotarod test is often used to assess locomotor coordination in rodents. In addition, the test can be modified for four consecutive days to enable a further demonstration of motor skill learning, which more likely reflects the vulnerability of DA depletion (17, 18). As previously reported (19), a decrease of locomotor activity was noticed in old male mice in comparison to young male ones, validating the specificity of the test. However, no significant difference of falling latency was found between WT and cKD mice within four trials, regardless of sex and age (Fig. 1E-H). In addition, no difference of grip strength was found (Supplemental Fig. S1C). Taken together, these results suggest that conditional knockdown of JMJD3 specifically affects chronic pain maintenance rather than locomotor coordination.

DA contents are decreased in cKD mouse midbrain and striatum.

To understand the biological alterations in JMJD3-deficient mouse brain, the levels of two catecholamines DA and NE were measured by high performance liquid chromatography-mass spectrometry (HPLC-MS) in several TH-enriched brain regions of young WT and cKD mice. The results demonstrated that the levels of DA in the midbrain and striatum of CKD mice were significantly lower than those of WT mice in both sexes, whereas no significant difference was observed in frontal cortex, cerebellum and brainstem (Fig. 2A and Supplemental Fig. S2A). By contrast, the level

of NE was not altered in any brain regions examined (Fig. 2B and Supplemental Fig. S2B), suggesting that the JMJD3 knockdown effect was confined to midbrain DA system.

To confirm the results above, a brain-penetrating JMJD3 inhibitor GSK-J4 (20) was daily injected intra-peritoneally into young male mice for five days, following by the same experimental procedure of HPLC-MS. Consistent with transgenic JMJD3 knockdown, decreased levels of DA but not NE were specifically observed in the midbrain and striatum of GSK-J4-injected mouse brains (Fig. 2C,D). These results provide consistent evidence supporting the vulnerability of midbrain DA contents to JMJD3 activity.

TH expression is decreased in midbrain DA neurons of cKD and GSK-J4 mice.

The biochemical findings above suggested that the DA biosynthesis in midbrain DA neurons might be affected by JMJD3. Thus, we examined the TH protein expression in the midbrains of young male WT and cKD mice by immunofluorescence microscopy analysis. We found that both the TH immunoreactivity and cell number of TH-positive DA neurons were significantly lower in the SNc and VTA of cKD mice in comparison to WT (Fig. 3A, B). Similarly, TH immunoreactivity was also decreased in the SNc and VTA of GSK-J4-injected mice, whereas no significant difference of total TH-positive cell number in either region was observed (Fig. 3C, D). It is worth mentioning that the decrease of TH-positive cell number is more likely resulted from the attenuated TH expression rather than the loss of DA neurons *per se*, as neither the total amount of cells nor the overall morphology in midbrain seems not altered (data not shown). Collectively, these results suggest that defect of TH

expression in midbrain DA neurons underlie JMJD3 deficiency-induced region-specific loss of DA contents.

JMJD3 epigenetically activates *Th* transcription in midbrain DA neurons.

JMJD3 is known as an epigenetic transcription activator. Thus, the transcription of *Th* gene across different brain regions was examined by real-time PCR analysis. We found a midbrain-specific decrease of both *Jmjd3* and *Th* mRNA level in cKD mice (Fig. 4A), suggesting that *Th* gene was transcriptionally regulated by JMJD3. To understand the underlying mechanism, primary culture of mouse midbrain DA neurons was challenged with GSK-J4 for 1 day and a dose-dependent decrease of TH-positive cell number was observed (Fig. 4B), together with a down-regulation of *Th* gene expression (Fig. 4C). Similar results were seen in a GSK-J4-treated DA neuronal cell line which consistently expressing TH (21) (Supplemental Fig. S3). To confirm the specificity of GSK-J4, we performed short hairpin RNA-mediated JMJD3 knockdown (sh-JMJD3) in primary DA neuron culture and observed similar results (Fig. 4D, E). These results demonstrate that JMJD3 is an essential positive regulator for *Th* gene transcription in midbrain DA neurons.

As a chromatin modifier, JMJD3 binds to DNA and specifically de-methylates H3K27 tri-methylation. By using chromatin immunoprecipitation assay, we found that GSK-J4 induced region-specific H3K27 tri-methylation within 1 kilo bp of *Th* gene promoter (Fig. 4F). Moreover, JMJD3 was specifically enriched within -750 to -450 bp of *Th* promoter, and its enrichment was remarkably decreased after GSK-J4 treatment (Fig. 4G). These results demonstrate that JMJD3 binds to *Th* promoter and erases the repressive histone modification mark for the transcription of *Th* gene.

Our study report a previously unknown role of JMJD3 for the DA synthesis in adult mouse midbrain DA neurons, and establish a connection of this cell type-specific deficiency with chronic pain. Recent studies have reported chronic pain as an inducer of DA content decrease in midbrain particularly VTA DA neurons (3, 5, 22). Evidence also exist suggesting that TH-expressing cells from other regions in central nervous system, such as A11 hypothalamic DA neurons and dorsal root ganglion neurons expressing C-low threshold mechanoreceptors (8, 23, 24). However, we found no significant difference of the DA level and TH expression in hypothalamus between WT and cKD mice (data not shown), and JMJD3 expression is almost undetectable in TH-expressing dorsal root ganglion neurons (unpublished data). Therefore, we conclude that the contributions of these regions to JMJD3-related DA deficiency and hyperalgesia, if any at all, are not comparable to that of midbrain DA neurons.

Our finding reveals that *Th* gene transcription is under epigenetic control of JMJD3 in midbrain DA neurons, indicating that the DA content reduction is cell autonomous. Importantly, midbrain DA neurons are not lost in cKD mice, demonstrating a non-toxic repression of TH and DA, which is distinguished from the neurotoxic characteristics commonly found in PD (25). Another discrepancy is that the decreased TH activity in SNc does not cause motor abnormalities similar to those in PD, as evidenced by no difference between cKD and WT mice in the performance of accelerating rotarod. The physiological roles of JMJD3-mediated regulation of DA synthesis in normal midbrain DA neurons remain to be further studied.

A high consistency of neurotransmitter content changes is observed between drug-induced global JMJD3 inhibition and DA neuron-specific JMJD3 knockdown. Recent studies suggest promising potential of JMJD3 inhibitors in cancer therapy. For instance, GSK-J4 exhibits high efficiency in targeting pediatric brainstem glioma and high-risk neuroblastoma (26, 27). However, our result shows that intra-peritoneal injection of GSK-J4 for 5 days would have remarkable impact on the metabolism of DA system in brain. This raises concerns about the adverse effects on DA-related functions and behaviors in pre-clinical and clinical trials with JMJD3 as therapeutic target.

Materials and Methods

Ethics

All animal experiments were approved by the animal ethics committee of Shanghai University of Medicine and Health Sciences and have been performed in accordance with the ethical standards laid down in the 1964 Declaration of Helsinki and its later amendments.

Animals

For pharmaceutical JMJD3 inhibition experiments, 4-month-old male C57BL/6 mice were purchased from Shanghai Jiesijie Experimental Animal Co. GSK-J4 dissolved in dimethyl sulfoxide (DMSO) was daily injected intraperitoneally at 20 mg/kg body weight into mice for five consecutive days. In parallel, DMSO was injected in the same manner as control. For TH-specific JMJD3 knockdown experiments, *Th*-CRE mice were crossbred with heterozygous floxed JMJD3 mice (a kind gift from Dr. Degui Charlie Chen) to generate cKD mice, whereas littermates of *Th*-CRE were used as WT. All animals were housed under standard conditions with controlled 12-hour light/dark cycles with food and water provided ad libitum.

Cell culture

Primary midbrain DA neurons were cultured as previously described (15) with minor modifications. DA progenitors were extracted from embryonic day 11 ICR mouse ventral mesencephalon. At this stage, the SNc and VTA are not anatomically or molecularly distinct (28, 29), enabling these cells differentiating into both DA subtypes. Briefly, progenitors were mechanically dissociated into single cells and plated onto 24-well plates or 6-well dishes pre-coated with 15 μg/ml poly-L-ornithine

and 1 μg/ml fibronectin. Cells were cultured in serum-free Neurobasal media supplemented with N2 and B27 supplements and 1% Penecillin/Streptomycin for 7 days to reach a complete DA neuronal differentiation. After that, GSK-J4 or DMSO were treated for 24 hours. MES23.5 cells were cultured in DMEM supplemented with 10% fetal bovine serum and 1% Penecillin/Streptomycin. All cells were incubated in 5% CO_2, 37 °C incubator.

Real-time PCR analysis

RNAs were extracted from cultured cells and tissues using RNA extraction kit and reverse transcribed into cDNAs (both from TAKARA) according manufacturers' instructions. Real-time PCR was performed on a Real-time system (Roche) using SYBR green supermix (Vazyme). The comparative cycle threshold method was used for quantification. Gene expression values were normalized to those of *Gapdh*. Primer sequences are listed in Supplemental Table S1A.

Fluorescence immunostaining analysis

Brain tissues were pre-fixed with 4% paraformaldehyde by cardiac perfusion and post-fixed for 3 hours, dehydrated in 30% sucrose and stored in embedding compound (Tissue-Tek) at -70°C until cryosection. Tissues were cryosectioned into 14 μm thickness (Leica CM1950). Cultured cells were fixed with 4% paraformaldehyde for 20 mins. For immunostaining, tissue slices or cultured cells were permeabilized and blocked with PBS with 0.3% TritonX-100 and 1% bovine serum albumin for 40 mins, incubated with mouse anti-TH primary antibody (Sigma) diluted with blocking solution at 4°C overnight. Alexa Fluor series of second antibodies (Thermo Scientific) were applied for one hour at room temperature. Cells were finally counterstained with

4',6-diamidino-2-phenylindole (DAPI) and examined using fluorescence microscope (Leica DMi8).

HPLC-MS analysis

HPLC-MS experiments were performed as previously described (30, 31). Briefly, samples from different brain regions after mouse sacrifice were homogenized in ice-cold 0.2M perchloric acid/methanol, sonicated (Bioruptor) and centrifuged at 10000 g for 20 mins. Supernatants were then filtered through 0.22 μm filter and stored in -80°C. At least four animals per genotype or drug treatment were used. Analytes were separated using a Model 1260 HPLC system consisting of a binary pump, on-line degasser, thermostated dual 54-well plate autosampler, and a thermosated column compartment (Agilent Technologies, Santa Clara, CA) with a Poroshell 120 SB-C18 reverse phase column (3.0x100 mm, 2.7 μm, particle size, Agilent Technologies, Santa Clara, CA) temperature-controlled at 25 □. The mobile phase consisted of A (1mM ammonium formate, 0.1%(v/v) formic acid and 1%(v/v) methanol in water) and B (1 mM ammonium formate 0.1%(v/v) formic acid and 0.9%(v/v) H2O in methanol). The gradient conditions of the mobile phase were as follows: 0 min, 5% B; 20 min,95% B; 21 min, 5% B and 28 min, 5% B. The flow rate of the mobile phase was 0.3 ml/min, and the injection volume was 10μl. For MS analysis, LC flow was coupled to an Agilent model 6470 triple quadrupole (QqQ) MS (Agilent Technologies, Santa Clara, CA), equipped with an Agilent Jet Stream (AJS) electrospray ionization (ESI) source. The mass spectrometer was operated with the following parameters: capillary voltage, 4000 V for positive and 3500 V for negative; nozzle voltage, 500 V. Nitrogen was used as the drying (5 L/min, 300 ℃), sheath (11 L/min, 250 ℃) and nebulizer gas (45 psi). The data was acquired using Agilent

MassHunter Workstation Data Acquisition Software (revision B.04). Multiple-reaction-monitoring transitions parameters, such as precursor ions, product ions, fragmentor voltage, collision energy (CE) as well as polarity were shown in Supplemental Table S1. For the compounds which had two product ions, it was shown that the product ion was used as quantitative ion or qualitative one in Supplemental Table S1B. The dwell time was 50 ms for transitions.

Mechanical hyperalgesia test

CFA-induced chronic mechanical hyperalgesia was assessed as previously described (32). Briefly, baseline responses were measured using von Frey's hairs (bending force range from 0.02-1.4 g, starting with 0.16g; Stoelting) after mice were placed on a wire grid without receiving any nociceptive stimulation for 2 hours. Next day, 20 μl CFA (Sigma-Aldrich) was injected intraplantarly, and the hyperalgesia responses were measured for various time points within 18 days. The hair force was increased or decreased according to the response, and the 50% paw withdrawal threshold was calculated using the up and-down method (33). Nociceptive responses include clear paw withdrawal, shaking, and licking. Stimulus and measurement were repeated if ambiguous responses such as ambulation occurred.

Hargreaves test

Thermal algesia to noxious stimulus was measured using a hot/cold plate analgesia meter for mice (IITC) according to manufacturer’s instructions. mice were put on a glass plate and the hind paw plantar surface was exposed to a beam of radiant heat (intensity latency 8-12 s) according to the Hargreaves method (16). Latencies of hind paw withdrawal were recorded. The heat stimulation was repeated 2 times at an

interval of 5 min for each mouse and the mean of both paws was calculated.

Grip strength test

Hindlimb grip strength was measured with a grip strength meter for mice consisted of a T-shaped metal bar connected to a force transducer (IITC). Briefly, mice were held by tails allowing them to grasp the metal bar with hind paws, followed by a pulling of the mice backwards by the tail until grip was lost. The peak force was automatically recorded in grams (g) by the device. The measurement of grip strength was repeated 5 times at an interval of 5 min for each mouse and the mean was calculated.

Accelerating rotarod test

The test was performed on a rotarod apparatus (IITC) according to manufacturer's manual. The 3 cm-diameter suspended rod was set to accelerate at a constant rate from 5 to 45 rpm in 240 s. Mice were pre-trained for 2 consecutive days before first trial. At each trial, mice were placed on the rod for a session of two repeats, with 180 s resting time allowed in between. A trial ended when the mouse fell off the rotarod or after reaching 240 s. The falling time was recorded and averaged of two repeats. Total four trials were performed for four consecutive days.

Cell counting and statistics

For in vivo immunoreactivity analysis, at least 50 TH-positive cells were counted in each brain region for one animal. Data were derived from three mouse brains of same experimental group and expressed as mean ± SEM. For in vivo TH-positive cell number analysis, the total number of TH-positive cells from sagittal sections containing VTA and SNc in one mouse brain was counted. To compensate the double

counting in adjacent regions, the Abercrombie correction factor was introduced as following: [N=n X (T/T+D)], in which N is the actual number of cells, n is the number of nuclear profiles, T is the section thickness, and D is the average diameter of nuclei. For in vitro analysis, cultured cells were counted in at least 10 random regions of each culture coverslip using an eyepiece grid at a magnification of 200 or 400X. Data are expressed as mean ± SEM of three independent cultures. For HPLC-MS analysis, data were derived from four to seven mouse brains of same transgenic background and expressed as mean ± SEM. Statistical comparisons were made using Student's t-test, one-way ANOVA with Tukey's post hoc analysis and two-way ANOVA with Sidak's multiple comparisons test (Graphpad Prism).

Competing Interest Statement

The authors declare no competing interests.

Acknowledgements

We thank Dr. Degui Charlie Chen for providing *Jmjd3* loxP mice. X.B.H. is supported by the National Natural Science Foundation of China (31701287). F.G. is supported by the National Natural Science Foundation of China (32100779).

Author Contributions

X.B.H. conceived the study, performed the experiments, generated figures and wrote the paper. W.Z. performed HPLC-MS and drafted the manuscript. F.G. performed the experiments, generated figures and drafted the manuscript. W.L. provided *Th*-CRE mice and provided administrative support. Y.Z., Y.M., Y.W. performed the experiments and generated figures. H.J.W. provided technical support for pain-related experiments. Q.Z. helped generate the mouse models. All authors have approved the final version of the manuscript.

References

1. Ossipov MH, Dussor GO, Porreca F. Central modulation of pain. *Journal of Clinical Investigation*. 2010;120(11):3779–3787.

2. Taylor AMW, et al. Mesolimbic dopamine signaling in acute and chronic pain: implications for motivation, analgesia, and addiction. *Pain*. 2016;157(6):1194–1198.

3. Yang H, et al. Pain modulates dopamine neurons via a spinal–parabrachial–mesencephalic circuit. *Nat Neurosci*. 2021;24(10):1402–1413.

4. Markovic T, et al. Pain induces adaptations in ventral tegmental area dopamine neurons to drive anhedonia-like behavior. *Nat Neurosci*. 2021;24(11):1601–1613.

5. Huang S, et al. Dopamine Inputs from the Ventral Tegmental Area into the Medial Prefrontal Cortex Modulate Neuropathic Pain-Associated Behaviors in Mice. *Cell Reports*. 2020;31(12):107812.

6. Martikainen IK, et al. Chronic Back Pain Is Associated with Alterations in Dopamine Neurotransmission in the Ventral Striatum. *Journal of Neuroscience*. 2015;35(27):9957–9965.

7. Scott DJ, et al. Variations in the Human Pain Stress Experience Mediated by Ventral and Dorsal Basal Ganglia Dopamine Activity. *Journal of Neuroscience*. 2006;26(42):10789–10795.

8. Hnasko TS, Sotak BN, Palmiter RD. Morphine reward in dopamine-deficient mice. *Nature*. 2005;438(7069):854–857.

9. Johnson ME, et al. Tyrosine hydroxylase as a sentinel for central and peripheral

tissue responses in Parkinson's progression: Evidence from clinical studies and neurotoxin models. *Progress in Neurobiology*. 2018;165–167:1–25.

10. Beiske AG, et al. Pain in Parkinson's disease: Prevalence and characteristics: *Pain*. 2009;141(1):173–177.

11. Lenartowski R, Goc A. Epigenetic, transcriptional and posttranscriptional regulation of the tyrosine hydroxylase gene. *Int j dev neurosci*. 2011;29(8):873–883.

12. van Heesbeen HJ, et al. Epigenetic mechanisms in the development and maintenance of dopaminergic neurons. *Development*. 2013;140(6):1159–1169.

13. Hong S, et al. Identification of JmjC domain-containing UTX and JMJD3 as histone H3 lysine 27 demethylases. *Proceedings of the National Academy of Sciences*. 2007;104(47):18439–18444.

14. Burchfield JS, et al. JMJD3 as an epigenetic regulator in development and disease. *The International Journal of Biochemistry & Cell Biology*. 2015;67:148–157.

15. He X-B, et al. Vitamin C Facilitates Dopamine Neuron Differentiation in Fetal Midbrain Through TET1- and JMJD3-Dependent Epigenetic Control Manner: Epigenetic Control of mDA Neuron Development by VC. *STEM CELLS*. 2015;33(4):1320–1332.

16. Hargreaves K, et al. A new and sensitive method for measuring thermal nociception in cutaneous hyperalgesia. *Pain*. 1988;32(1):77–88.

17. Chagniel L, et al. Partial dopamine depletion in MPTP-treated mice differentially altered motor skill learning and action control. *Behavioural Brain Research*.

2012;228(1):9–15.

18. Shiotsuki H, et al. A rotarod test for evaluation of motor skill learning. *Journal of Neuroscience Methods*. 2010;189(2):180–185.

19. Shoji H, et al. Age-related changes in behavior in C57BL/6J mice from young adulthood to middle age. *Molecular Brain*. 2016;9(1). https://doi.org/10.1186/s13041-016-0191-9

20. Kruidenier L, et al. A selective jumonji H3K27 demethylase inhibitor modulates the proinflammatory macrophage response. *Nature*. 2012;488(7411):404–408.

21. Crawford GD, et al. A novel N18TG2 x mesencephalon cell hybrid expresses properties that suggest a dopaminergic cell line of substantia nigra origin. *Journal of Neuroscience*. 1992;12(9):3392–3398.

22. Vergara F, et al. Contribution of mesolimbic dopamine and kappa opioid systems to the transition from acute to chronic pain. *Neuropharmacology*. 2020;178:108226.

23. Brumovsky PR. Dorsal root ganglion neurons and tyrosine hydroxylase—an intriguing association with implications for sensation and pain: *PAIN*. 2016;157(2):314–320.

24. Seal RP, et al. Injury-induced mechanical hypersensitivity requires C-low threshold mechanoreceptors. *Nature*. 2009;462(7273):651–655.

25. Meredith GE, Sonsalla PK, Chesselet M-F. Animal models of Parkinson's disease progression. *Acta Neuropathol*. 2008;115(4):385–398.

26. Hashizume R, et al. Pharmacologic inhibition of histone demethylation as a therapy for pediatric brainstem glioma. *Nature Medicine*. 2014;20(12):1394–1396.

27. Lochmann TL, et al. Targeted inhibition of histone H3K27 demethylation is effective in high-risk neuroblastoma. *Sci Transl Med*. 2018;10(441):eaao4680.

28. Hu Z, et al. Differentiation of the midbrain dopaminergic pathways during mouse development. *J Comp Neurol*. 2004;476(3):301–311.

29. La Manno G, et al. Molecular Diversity of Midbrain Development in Mouse, Human, and Stem Cells. *Cell*. 2016;167(2):566-580.e19.

30. Pu T, et al. An in vitro DNA phosphorothioate modification reaction. *Mol Microbiol*. 2020;113(2):452–463.

31. Sun W, et al. Natural variation and underlying genetic loci of γ-oryzanol in Asian cultivated rice seeds. *The Plant Genome*. [published online ahead of print: June 27, 2022]; https://doi.org/10.1002/tpg2.20201

32. Wang H, et al. Balancing GRK2 and EPAC1 levels prevents and relieves chronic pain. *J Clin Invest*. 2013;123(12):5023–5034.

33. Chaplan SR, et al. Quantitative assessment of tactile allodynia in the rat paw. *Journal of Neuroscience Methods*. 1994;53(1):55–63.

Figure Legends

Figure 1. Tyrosine hydroxylase-specific JMJD3 knockdown affects inflammation-induced mechanical hyperalgesia but not locomotor functions. (A-D) Conditional knockdown (cKD) mice and their control littermates (WT) received an intraplantar injection of complete Freund's adjuvant and changes in 50% paw withdrawal threshold assessed by Von Frey's hair were monitored over 18 days. Mice were grouped into young (4-6 months old (mo); A, B) and old (12-14 mo; C, D), male (A, C) and female (B, D). (E-H) In parallel, mice underwent the accelerating rotarod test daily for four consecutive days. The falling time of each mouse was averaged of two repeats. Data represent mean ± SEM. $*P < 0.05$, $**P < 0.01$, $****P < 0.0001$; two-way ANOVA with Sidak's multiple comparisons test.

Figure 2. Dopamine levels are decreased in the midbrain and striatum of two mouse models of JMJD3 deficiency. Brain tissues from frontal cortex (CTX), striatum (STRM), midbrain (MB), cerebellum (CB) and medulla oblongata (MO) were micro-dissected, homogenized and the contents of dopamine (DA) and norepinephrine (NE) were measured by high performance liquid chromatography-mass spectrometry. (A, B) 4-month-old male conditional knockdown (cKD) mice and their control littermates (WT). (C, D) 4-month-old male C57BL/6 mice underwent 5 consecutive days of intra-peritoneal injection of GSK-J4 (20mg/kg daily). In parallel, dimethyl sulfoxide was injected as Vehicle. N= 4-7 mice. Data represent mean ± SEM. $*P < 0.05$, $****P < 0.0001$; Student's t-test.

Figure 3. Decreased tyrosine hydroxylase expression in midbrain dopamine neurons of two JMJD3 deficiency models. (A) Schematics of mouse midbrain

compromised of ventral tegmental area (VTA), substantia nigra pars compacta (SNc) and pars reticulata (SNr). Dotted lines a-d in coronal view and box in sagittal view indicate positions shown in B and D. (B) Representative immunofluorescence images of tyrosine hydroxylase (TH)-positive midbrain dopamine (DA) neurons in conditional knockdown (cKD) mice and their control littermates (WT). (C) Quantification of TH immunoreactivity and cell number of DA neurons in VTA and SNc in WT and cKD mice. (D) Representative immunofluorescence images of TH-positive DA neurons in GSK-J4 injected mice and their control (Vehicle). (E) Quantification of TH immunoreactivity and cell number of DA neurons in VTA and SNc in GSK-J4 injected mice and control. For immunoreactivity analysis, at least 50 TH-positive cells were measured and the mean was calculated for one mouse. N = 3-5 mice. Data represent mean ± SEM. $*P < 0.05$, $**P < 0.01$, $****P < 0.0001$; Student's t-test. Scale bar represents 100 μm.

Figure 4. Epigenetic control of *Th* gene transcription by JMJD3. (A) Real-time PCR analysis of mRNA levels of *Jmjd3* and *Th* from different brain regions in conditional knockdown mice (cKD) and their control littermates (WT). Note that both genes are specifically down-regulated in striatum (STRM) and midbrain (MB), but not frontal cortex (CTX), cerebellum (CB) or medulla oblongata (MO). N = 3 mice. Data represent mean ± SEM. (B) Representative immunofluorescence images of tyrosine hydroxylase (TH)-expressing dopamine (DA) neurons and cell number quantification in primary mouse DA neuronal cell culture with or without treatment of GSK-J4. Scale bar represents 100 μm. (C) *Th* mRNA level in primary DA neuronal culture after GSK-J4 treatment. (D) Quantification of TH+ cell number in primary mouse DA neuronal cell culture underwent short hairpin RNA-mediated JMJD3

knockdown (sh-JMJD3) or control (plko.1). (E) mRNA levels of *Jmjd3*, *Utx* and *Th* affected by sh-JMJD3. (F) Chromatin immunoprecipitation (ChIP)-qPCR analysis of histone 3 lysine 27 tri-methylation (H3K27me3) on 1 kilo bp mouse *Th* promoter region from primary DA neuronal cell samples with or without GSK-J4 treatment. (G) ChIP-qPCR analysis showing altered enrichment of JMJD3 on a specific region of mouse *Th* promoter by GSK-J4. N = 3 independent cell cultures. Data represent mean ± SEM. *$P < 0.05$; Student's t-test and one-way ANOVA with Tukey's post hoc test.

Supplemental Figure Legends

Supplemental Figure S1. (A) Genotyping of JMJD3 conditional knockdown (cKD) mice. Genetic DNAs were extracted from tails of mice and applied to semi-quantitative PCR analysis to verify the loci carrying *Th*-CRE and *Jmjd3* loxP sequences using specific primers. Mice carrying one band by *Th*-CRE primer and two bands by loxP primer represent cKD and mice carrying one band by CRE primer and one band near 300 bp by loxP primer represent control genotype (WT). (B) Thermal hyperalgesia of cKD and WT mice in different sexes and ages were assessed by Hargreaves method. Latencies of hind paw withdrawal were recorded. (C) grip strength of cKD and WT mice in different sexes and ages were compared. Data represent mean ± SEM. Student's t-test.

Supplemental Figure S2. Dopamine (DA) and norepinephrine (NE) levels were measured by high performance liquid chromatography-mass spectrometry in five brain regions including frontal cortex (CTX), striatum (STRM), midbrain (MB), cerebellum (CB) and medulla oblongata (MO) from 4-month-old female conditional knockdown mice (cKD) and their control littermates (WT). N = 4-7 mice. Data represent mean ± SEM. $*P < 0.05$, Student's t-test.

Supplemental Figure S3. (A) Representative immunofluorescence images and quantification of tyrosine hydroxylase (TH)-positive cells in MES23.5 DA neuronal cell culture with or without treatment of JMJD3 inhibitor GSK-J4. Cell numbers were counted in 10 random areas of each culture coverslip using an eyepiece grid at a magnification ×100. Scale bar represents 100 μm. (B) Real-time PCR analysis of *Th* mRNA expression in response to different doses of GSK-J4 treatment. N = 3

independent cell cultures. Data represent mean ± SEM. *$P < 0.05$; one-way ANOVA with Tukey's post hoc test.

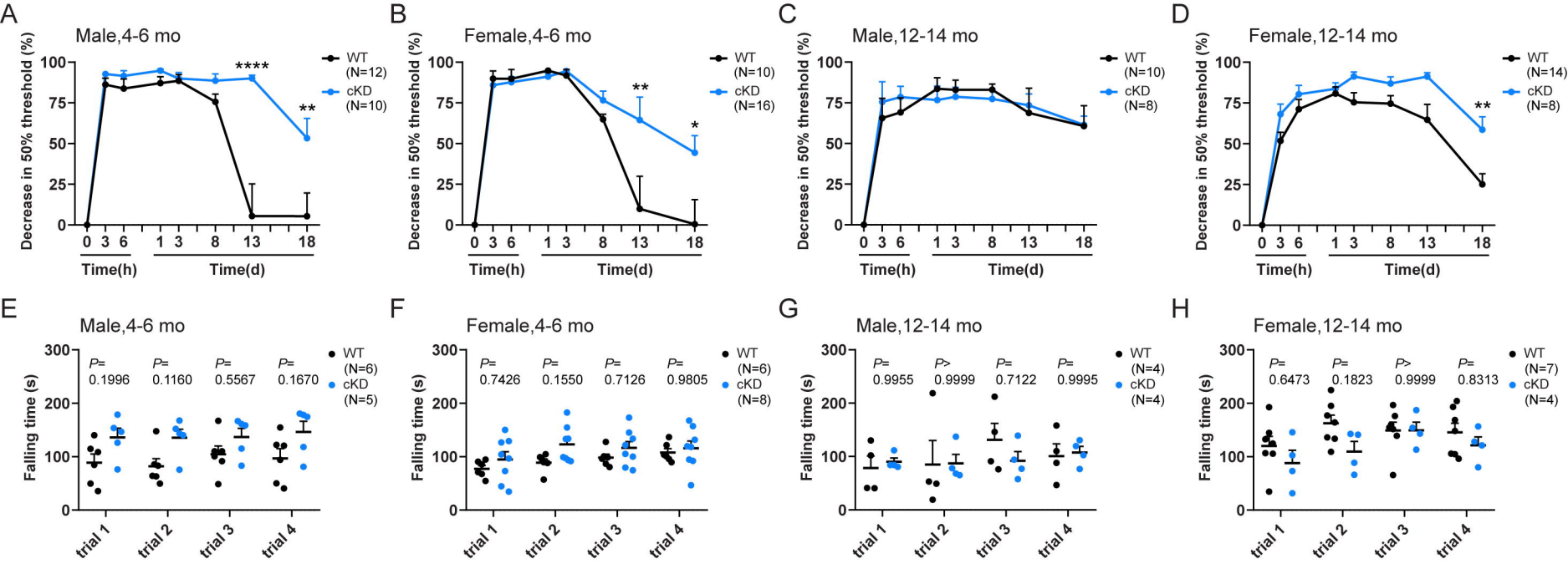
A
Male,4-6 mo
Decrease in 50% threshold (%)
100
75
50
25
0
****
**
WT (N=12)
cKD (N=10)
0 3 6
1 3 8 13 18
Time(h)
Time(d)
B
Female,4-6 mo
**
*
WT (N=10)
cKD (N=16)
C
Male,12-14 mo
WT (N=10)
cKD (N=8)
D
Female,12-14 mo
**
WT (N=14)
cKD (N=8)
E
Male,4-6 mo
Falling time (s)
300
200
100
0
P= 0.1996
P= 0.1160
P= 0.5567
P= 0.1670
WT (N=6)
cKD (N=5)
trial 1
trial 2
trial 3
trial 4
F
Female,4-6 mo
P= 0.7426
P= 0.1550
P= 0.7126
P= 0.9805
WT (N=6)
cKD (N=8)
G
Male,12-14 mo
P= 0.9955
P> 0.9999
P= 0.7122
P= 0.9995
WT (N=4)
cKD (N=4)
H
Female,12-14 mo
P= 0.6473
P= 0.1823
P> 0.9999
P= 0.8313
WT (N=7)
cKD (N=4)

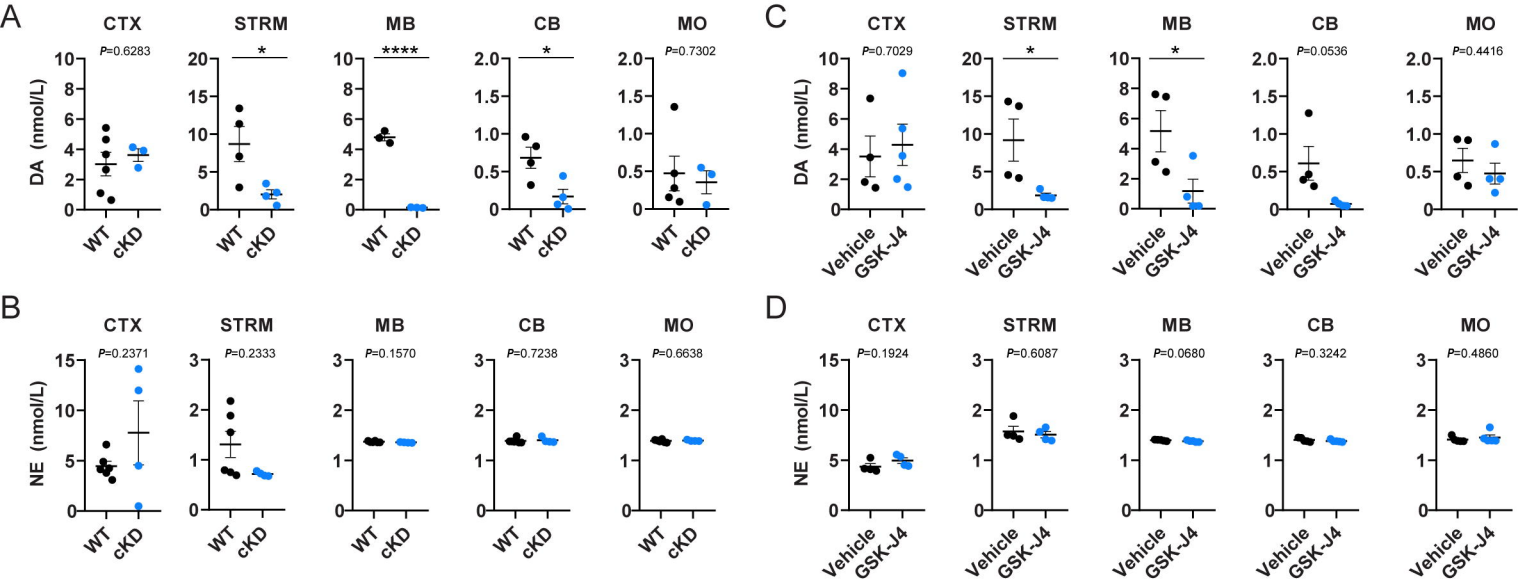
A
CTX
STRM
MB
CB
MO
DA (nmol/L)
P=0.6283
*
****
*
P=0.7302
WT
cKD
B
NE (nmol/L)
P=0.2371
P=0.2333
P=0.1570
P=0.7238
P=0.6638
C
P=0.7029
*
*
P=0.0536
P=0.4416
Vehicle
GSK-J4
D
P=0.1924
P=0.6087
P=0.0680
P=0.3242
P=0.4860

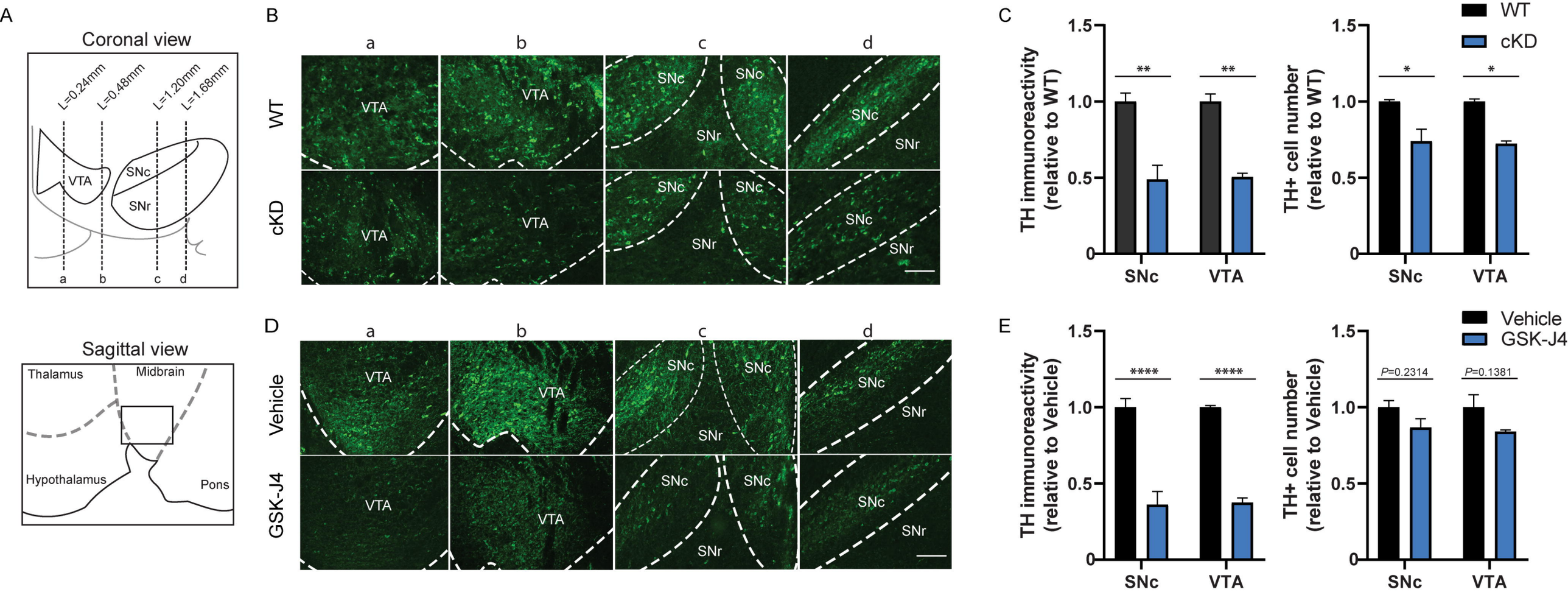
A
Coronal view
L=0.24mm
L=0.48mm
L=1.20mm
L=1.68mm
VTA
SNc
SNr
a
b
c
d
Sagittal view
Thalamus
Midbrain
Hypothalamus
Pons
B
a
b
c
d
WT
cKD
VTA
SNc
SNr
C
WT
cKD
TH immunoreactivity (relative to WT)
TH+ cell number (relative to WT)
1.5
1.0
0.5
0
**
*
SNc
VTA
D
Vehicle
GSK-J4
E
Vehicle
GSK-J4
TH immunoreactivity (relative to Vehicle)
TH+ cell number (relative to Vehicle)
****
P=0.2314
P=0.1381

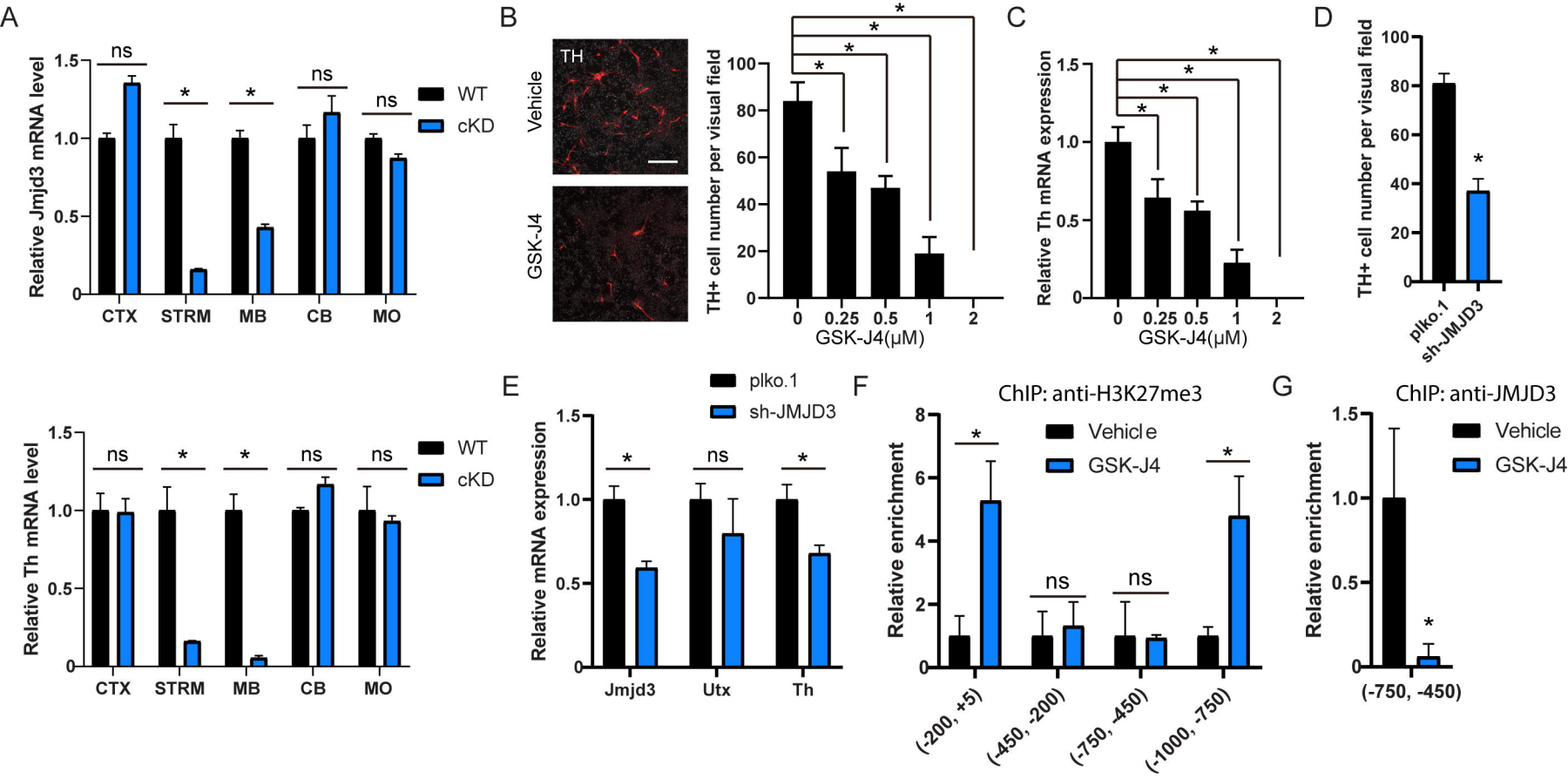
A
Relative Jmjd3 mRNA level
ns
*
*
ns
ns
WT
cKD
CTX
STRM
MB
CB
MO
B
TH
Vehicle
GSK-J4
TH+ cell number per visual field
GSK-J4(μM)
0
0.25
0.5
1
2
C
Relative Th mRNA expression
GSK-J4(μM)
D
TH+ cell number per visual field
plko.1
sh-JMJD3
Relative Th mRNA level
E
plko.1
sh-JMJD3
Relative mRNA expression
Jmjd3
Utx
Th
F
ChIP: anti-H3K27me3
Vehicle
GSK-J4
Relative enrichment
(-200, +5)
(-450, -200)
(-750, -450)
(-1000, -750)
G
ChIP: anti-JMJD3
Vehicle
GSK-J4
Relative enrichment
(-750, -450)